Phonons and phase stability in Ti-V approximants to gum metal

Y. Hanlumyuang, R. P. Sankaran, M. P. Sherburne, J. W. Morris, Jr., and D. C. Chrzan

Phys. Rev. B **85**, 144108 — Published 13 April 2012

DOI: 10.1103/PhysRevB.85.144108

Phonons And Phase Stability in Ti-V Approximants to Gum Metal

Y. Hanlumyuang, R. P. Sankaran, M.P. Sherburne,
J. W. Morris, Jr. , and D. C. Chrzan
Department of Materials Science and Engineering
University of California, Berkeley, California 94720, USA

The stability of competing phases within body-centered-cubic (bcc) Ti-V approximants to Gum Metal is considered from the perspective of the phonon dispersion. Phonons are associated with the potential to form the ω and α'' phases. It is argued that alloys can be designed to be linearly stable with respect to the formation of both phases, even as the ideal shear strength approaches zero. The reduction in ideal strength is associated with softening of the phonons along $\Gamma - N$, and is reflected in diffuse scattering diffraction experiments.

PACS numbers:

I. INTRODUCTION

Gum Metal is a body-centered-cubic (bcc) solid solution Ti-Nb based alloy that displays a large elastic limit, substantial elongation to failure, and high strength[1]. Further, these impressive properties emerge fully only after substantial cold work. Surprisingly, plastic deformation is not associated with obvious dislocation activity. These observations led Saito *et al.* to the remarkable conclusion that Gum Metal is a bulk, engineering alloy that deforms at its ideal strength[1]. If this conclusion is correct, Gum Metal represents a new type of structural alloy.

Of course, alloys can deform plastically via mechanisms other than the motion of dislocations. For example, applied stresses can trigger phase transformations that act so as to relieve the applied stress. In fact, Talling *et al.* considered the deformation of Gum Metal and concluded that the material deforms via a transformation from the so-called β-phase (bcc) to the face-centered-orthorhombic α''-phase[2]. This conclusion is supported by x-ray diffraction experiments showing reflections at positions that are normally associated with the α'' phase[3]. Further they propose that the formation of the α''-phase is linked to the formation of the ω-phase within the material. These experiments suggest that the plastic deformation mechanism in Gum Metal is not particularly novel.

However, Withey *et al.* studied the compression of nano-pillars of Gum Metal using *in situ* transmission electron microscopy[4]. These experiments enabled correlation of the appearance and intensity of diffracted beams associated with the α''-phase with the load versus displacement curve. During compression of nanopillars, the α''-phase appears, but it appears well before the maximum stress is reached. The intensity of the spot does not obviously grow with continued deformation, suggesting that the appearance of the α''-phase is incidental to the dominant plasticity mechanism. Further, an analysis of the energies associated with the transformation to the α''-phase suggests that Gum Metal is successfully engineered to suppress extensive transformation to this phase[5].

Theoretical work suggests how it might be possible for a bulk alloy to deform at ideal strength[6], and offers an explanation[7] for the lack of obvious dislocations and the formation of nanodisturbances[8] in deformed samples. Specifically, Gum Metal was designed with the intent to drive the elastic constant difference $C_{11} - C_{12} \to 0$. This design goal decreases the ideal strength of the alloy[1] and also increases the elastic anisotropy of the material. This anisotropy leads to directly the easy pinning[6] and large spreading[7] of dislocation cores. The large spreading, in turn, can yield nanodisturbances[8] through the overlap of dislocation cores.

Clearly, the relationship between elastic anisotropy, phase transformations, and the plastic deformation of Gum Metal remains an interesting area of exploration. Insight into the phase stability of the alloy can be obtained by considering the properties of phonons within the material. Here, a simple empirical model relating the phonon structure to the elastic anisotropy is explored and used to shed light on phase stability within Ti-V approximants to Gum Metal. While the simple calculations presented here employ parameters appropriate for Ti-V alloys, the trends so identified are likely to appear in Gum Metal as well. We expect, therefore, that the calculations will shed light on experimental results obtained through study of Gum Metal.

In what follows, it is shown that it is theoretically possible for a bcc alloy to be linearly stable with respect to the formation of both the ω and α'' phases even in the limit that its ideal shear strength approaches zero. Further, the reduction in ideal shear strength is accompanied by the softening of the phonons along $\Gamma - N$ (the Brillouin zone is shown in Fig. 1). This softening leads to spots in diffuse scattering experiments that coincide with those expected from the formation of a stable α'' phase. Finally, it is suggested that transformation to the hexagonal close packed (hcp) α phase via the Burgers path[9] leads to shear faults oriented as observed in experimental studies of solution treated Gum Metal[1].

II. PHONON MODEL

Computing the phonons within Gum Metal alloys poses substantial challenges (see, for example, ref.[10]). Here, the problem is simplified by employing a model that restricts contributions to the dynamical matrix to arise only from nearest and next nearest neighbor contributions. This restriction, when coupled with the average cubic symmetry of the alloy, defines the phonon dispersion relationship in terms of four parameters, the so called Born von Karman constants. By examining the long wavelength limit, these constants can be related to the elastic constants of the material. In the past, this model has been used successfully to study the transformation from the β-phase to the ω-phase[11].

Under the assumption of cubic symmetry and the restriction to first and second neighbor interactions, the dynamical matrix can be expressed in terms of four constants, α_1, γ_1, α_2 and β_2:[11]

$$\begin{aligned}\tilde{\Phi}_{11}(\mathbf{q}) &= 8\alpha_1\left(1-\cos\pi p_1\cos\pi p_2\cos\pi p_3\right)\\ &\quad+2\alpha_2\left(1-\cos 2\pi p_1\right)\\ &\quad+2\beta_2\left(2-\cos 2\pi p_2-\cos 2\pi p_3\right)\\ \tilde{\Phi}_{12}(\mathbf{q}) &= 8\gamma_1\sin\pi p_1\sin\pi p_2\cos\pi p_3.\end{aligned} \tag{1}$$

with $\mathbf{q} = (2\pi/a)(p_1, p_2, p_3)$ a reciprocal vector within the first Brillouin zone. The remaining components of the dynamical matrix can be found using cyclic symmetry.

Near $\mathbf{q} = 0$, the dynamical matrix can be expressed, in terms of the cubic elastic constants C_{11}, C_{12} and C_{44}:

$$\begin{aligned}\tilde{\Phi}_{11}(\mathbf{q}) &= \frac{a^3}{2}\left[C_{11}q_1^2 + C_{44}(q_2^2+q_3^2)\right]\\ \tilde{\Phi}_{12}(\mathbf{q}) &= \frac{a^3}{2}\left(C_{12}+C_{44}\right)q_1q_2.\end{aligned} \tag{2}$$

Matching Eqs. (1) to (2) as $\mathbf{q}\to 0$, one finds

$$\begin{aligned}2\alpha_1+2\alpha_2 &= aC_{11}\\ 2\alpha_1+2\beta_2 &= aC_{44}\\ 4\gamma_1 &= a(C_{12}+C_{44}).\end{aligned} \tag{3}$$

Equations (3) enable the study of the relationship between the elastic constants of the alloy, and the phonon frequencies. However, three elastic constants cannot determine uniquely four Born von Karman parameters. To define all four parameters, more information is needed.

Here, we employ TiV as an approximant to Gum Metal behavior. The elastic constants C_{11}, C_{12} and C_{44} are obtained from first principles total energy calculations for TiV alloys within the virtual crystal approximation[6]. A fourth equation is provided by a frozen phonon calculation[12] of the phonon frequency at H (Fig. 1). The frozen phonon data is obtained using the Quantum Espresso package[13], and the virtual crystal approximation for Ti-V alloys[6]. The energy cutoff of the frozen phonon calculations is chosen to be 1560 eV. A Fermi-Dirac smearing of 0.27 eV is employed. Energies are completely converged with respect to **k**-point sampling. Symmetrized Monkhorst-Pack grids are employed. For the H-point phonon, the unsymmetrized grid is $16\times16\times16$. As a check of the simple model, frozen phonon calculations are carried out for the N-point and the **q** associated with the ω phase. The unsymmetrized Monkhorst-Pack grids are $13\times13\times21$ and $18\times18\times11$ respectively. Energies are converged to better than 0.03 meV/atom.

In order to study trends as the bcc to hcp transition composition is approached from the bcc side, the phonon dispersion is computed as a function of composition using the Born von Karman constants. The resulting dispersion relations are plotted in Fig. 2, along with the predictions of the frozen phonon calculations. Note that the simple model computes the H-point frequency exactly. The agreement between the simple model and the frozen phonon predictions at N and the chosen point along the $P-H$ direction is an indication that the Born von Karman model is a reasonable model for phonons in the TiV alloys as described within the virtual crystal approximation.

III. DISCUSSION

Two anomalies are evident from the dispersion relations in Fig. 2: (1) The transverse mode close to (but not exactly at) $\mathbf{q} = \left(\frac{1}{3}, \frac{1}{3}, \frac{2}{3}\right)$ conincides with a dip in energy, and (2) the transverse branch from Γ to N with $[1\bar{1}0]$ polarization has an unusually low energy.

Consider first the transverse mode with the propagation vector close to $\mathbf{q} = \left(\frac{1}{3}, \frac{1}{3}, \frac{2}{3}\right)$. The lowest energy eigenvalue corresponds to the $(11\bar{1})$ polarization. This transverse mode is symmetrically equivalent to the longitudinal one with $\mathbf{q} = \left(\frac{2}{3}, \frac{2}{3}, \frac{\bar{2}}{3}\right)$. The atomic displacements along the $\langle ppp \rangle$ direction by this phonon mode result in two of the three neighboring (111) planes moving toward each other, whereas every third plane remains at rest. This structural transformation leads to the ω phase, hence this type of phonon is referred to as the $\mathbf{q}_\omega$ phonon. The same transformation mechanism has been reported in other bcc alloys[11].

The calculated total energy as a function of the displacement amplitude for $\mathbf{q} = \mathbf{q}_\omega$ frozen phonon for the composition $Ti_{25}V_{75}$, $Ti_{50}V_{50}$, and $Ti_{85}V_{15}$ is displayed in Fig. 3. The energy functions of $Ti_{25}V_{75}$ and $Ti_{50}V_{50}$ are close to parabolic near zero displacement, indicating nearly harmonic behavior. The calculated vibrational frequencies of these two compositions are close to the harmonic model as shown in Fig. 1. The energy rises sharply in the direction of oscillation away from the ω structure, while on the other side it rises to a local maximum at the amplitude of ~ 0.45 Å, required for ω-phase formation. The ω phase in $Ti_{85}V_{15}$ is just barely stable within our calculation. More sophisticated treatments of phase stability suggest that within Ti_3Nb alloys, the β phase is stabilized by thermal effects[10]. Irrespective, the energy-amplitude relations indicate that the ω phase is linearly unstable in these TiV approximants to Gum Metal.

The softening of phonons along the $\Gamma - N$ direction holds implication for diffraction experiments. By stacking two adjacent Brillouin zones as in Fig. 1, it is clear that the transverse N-point phonon mode is also equivalent to the $\mathbf{q} = (\frac{1}{2}, \frac{1}{2}, 1)$ mode with the [110] polarization. The dispersion relation at the points of type $(m/2, m/2, m)$, where m is an odd integer can be seen on the (110) section of the $q-$space.

To examine the diffraction pattern experimentally, a sample of Gum Metal fabricated and processed (cold-swaged, then solution treated at 900 C for 30 minutes) by Toyota Central Research and Development Laboratories, with composition 73.1Ti-23Nb-0.7Ta-2Zr-1.2O (at. %) was cut, polished using 4000 grit abrasive, and disc cut. The sample was then electropolished in a Fischione 1010 jet polisher, using a 4.6% perchloric acid in methanol and butanol solution at 40 mA, 35 V and at -30 C. The transmission electron diffraction pattern from this sample was then obtained using a JEOL 2011 electron microscope. The diffraction pattern is shown in Fig. 4(c). The brightest spots, shown indexed by integers, are those expected from the bcc structure. In addition, however, there are additional reflections that appear at spots normally associated with the α''-phase (*e. g.* the spot indexed by $\frac{1}{2}\,\frac{\bar{1}}{2}\,1$, and symmetry related spots). One explanation for these spots is that the sample includes a volume of the α''-phase.

However, it is possible that the lower intensity excitations at $\mathbf{q} = (\frac{1}{2}, \frac{\bar{1}}{2}, 1)$ are a result of the softening of the N-point phonon. This possibility becomes more likely, given that dark field imaging yields no evidence for the hcp phase. To investigate this possibility, the theoretical intensity of diffraction patterns of phonon scattering are computed. The intensity obtained from the thermal average of the displacement fluctuations is given by

$$I(\mathbf{q}) = I_o(\mathbf{q}) + I_1(\mathbf{q}) + \dots \tag{4}$$

where

$$\begin{aligned} I_o(\mathbf{q}) =& N e^{-2W(\mathbf{q})} \sum_R e^{i\mathbf{q}\cdot\mathbf{R}} \\ I_1(\mathbf{q}) =& \frac{N}{m} e^{-2W(\mathbf{q})} \sum_r |\mathbf{q}\cdot\mathbf{a}_r(\mathbf{q}-\mathbf{G})|^2 \, \frac{\langle E_r(\mathbf{q}-\mathbf{G})\rangle}{\omega_r^2(\mathbf{q}-\mathbf{G})} \end{aligned} \tag{5}$$

Here, the average energy of a single oscillator is $\langle E_r(\mathbf{q})\rangle = (\hbar\omega/2)\coth(\hbar\omega/2k_BT)$. The index $r = 1, 2, 3$ labels the polarization of the phonon mode, and $W(\mathbf{q})$ is the Debye-Waller factor[14]. Higher order terms are neglected here, as they contribute intensities at the level of a few percent of the first order term.

The theoretical first-order intensities on the $(1\bar{1}0)$ section are displayed in Fig. 4 for both $Ti_{25}V_{75}$ and $Ti_{85}V_{15}$. The intensity scale is set equal for both Figs. 4(a) and 4(b). The similarity between Figs. 4(b) and 4(c) are strong, especially if one allows for the simplicity of the diffraction model. The calculations make clear that phonons within a stable bcc crystal structure can lead to diffuse scattering at the positions in reciprocal space expected from a stable α''-phase. Further, phonons alone lead to streaking similar to that observed experimentally. Both the diffuse spots and the streaking become more intense for $Ti_{85}V_{15}$ as compared with $Ti_{25}V_{75}$. Based on these observations, it is possible that the experimental observation of the α'' phase is actually the observation of softening phonons within the stable bcc phase.

It is insightful to examine the structures arising from the soft phonons at N. The fluctuations at the $N-$point result in displacements of two neighboring (110) plane in opposite $[1\bar{1}0]$ direction as shown in Fig. 5(a). Viewing along the [110] direction, the $N-$point phonon leads to a structure close to hexagonal. The angle between the atomic bonds in the basal plane are 109.47° and 125.27°. The precise 120° angles required for forming a hcp structure

can be achieved by applying a simple shear close to the type $[\bar{1}11](1\bar{1}2)$ as shown in Fig. 5(b). This mechanism was discovered by Burgers[9].

The shear angle and magnitude required to convert the bcc phase into hcp can be obtained solely from geometry. More specifically, one chooses the shear angle and magnitude so that the angles θ_1 and θ_2 become $2\pi/3$. The simple shear transformation tensor $\mathbf{F}_\gamma$ is given by

$$\mathbf{F}_\gamma = \begin{pmatrix} 1 & \gamma & 0 \\ 0 & 1 & 0 \\ 0 & 0 & 1 \end{pmatrix}. \tag{6}$$

Setting $\gamma = 0.20308$,taking the shear direction to coincide with the solid arrow in Fig. 5(b), and applying the transformation converts the bcc structure to a hexagonal one. The shuffling of every other plane leads to the hcp structure.

Interestingly, the orientation of this shear nearly coincides with the orientation of the shear bands observed by Saito et al.[1] during the deformation of solution treated Gum Metal. Hence it seems reasonable to associate this deformation with the localized transformation to the hcp phase, and suggests that the elastic limit, at least in some circumstances, is defined by this shear. This observation is consistent with the predicted softness of the N-point phonons.

The softening of the phonons along the $\Gamma - N$ branch is apparent in other contexts. For example, the displacements predicted in calculations of dislocation core structures are similar to those arising from these soft phonons[7]. Interestingly, there is experimental evidence for the softening of similar phonons in potassium, a material identified in[7] as one with elastic anisotropy similar to that of Gum Metal. Low energy electron diffraction experiments of the $\{110\}$ surface revealed the signature of large shears of the surface layer relative the bulk. Electronic structure calculations suggested that force constants governing the shear of the surface layers were so small that zero point motion alone could account for the experimental observations[15,16].

IV. CONCLUSION

In conclusion, phonon dispersion relations, obtained from the harmonic model in conjunction with first principles calculations provide insights into potential structural transformation in Gum Metals. The ω phase is a result of a soft longitudinal phonon with the wavevector $\mathbf{q} = (2/3, 2/3, 2/3)$. The transformation to the α''-phase is associated with a transverse $N-$point phonon. However, the alloys can be designed so that they are linearly stable with respect to the formation of both phases. Further, even though the bcc structure is linearly stable, the softening of the phonons can lead to diffuse scattering in diffraction experiments. Theoretical predictions for this diffuse scattering give patterns similar to those observed during electron diffraction experiments exploring solution treated Gum Metal.

V. ACKNOWLEDGMENT

The authors acknowledge the support of the National Science Foundation under Grant Nos. DMR-0706554, DMR-1105081 and Toyota Research and Development. This research used resources of the National Energy Research Scientific Computing Center, that is supported by the Office of Science of the U.S. Department of Energy under Contract No. DE-AC02-05CH11231.

[1] T. Saito, T. Furuta, J. H. Hwang, S. Kuramoto, K. Nishino, and et al. N. Suzuki. *Science*, 300:464, 2003.
[2] R. J. Talling, M. Jackson, R. J. Dashwood, S. Kuramoto, and D. Dye. *Scripta Mater.*, 59:669, 2008.
[3] R. J. Talling, R. J. Dashwood, M. Jackson, and D. Dye. *Acta Mat.*, 57:1188, 2009.
[4] E. A. Withey, A. M. Minor, D. C. Chrzan, J.W. Morris, Jr., and S. Kuramoto. *Acta Mater.*, 58:2652, 2010.
[5] J W Morris Jr., Y. Hanlumyuang, M. Sherburne, E. Withey, D. C. Chrzan, S. Kuramoto, Y. Hayashi, and M. Hara. *Acta Mat.*, 58:3271, 2010.
[6] T. Li, J.W. Morris, Jr., N. Nagasako, S. Kuramoto, and D. C. Chrzan. *Phys. Rev. Lett.*, 98:105503, 2007.
[7] D. C. Chrzan, M. P. Sherburne, Y. Hanlumyuang, T. Li, and J.W. Morris, Jr. *Phys. Rev. B*, 82:184202, 2010.
[8] M. Y. Gutkin, T. Ishizaki, S. Kuramoto, and I. A. Ovid'ko. *Acta Mater.*, 54:2489, 2006.
[9] W. G. Burgers. *Physica (Amsterdam)*, 1:561, 1934.
[10] Peter Lazar, Michal Jahnatek, Jürgen Hafner, Naoyuki Nagasako, Ryoji Asahi, Claudia Blass-Schenner, Markus Stöhr, and Raimund Podloucky. Temperature-induced martensitic phase transitions in gum-metal approximants: First-principles investigations for ti_3nb. *Physical Review B*, page 054202, 2011.
[11] D. De Fontaine. *Acta Met.*, 18:275, 1970.
[12] K. M. Ho, C. L. Fu, and B. N. Harmon. *Phys. Rev. B*, 29:1575, 1984.
[13] P. Giannozzi, S. Baroni, N. Bonini, and et. al. *J. of Phys. Cond. Matt.*, 21:395502, 2009.
[14] A. A. Maradudin, E.W. Montroll, and G. H. Weiss. *Theory of Lattice Dynamics in The Harmonic Approximation*. Academic Press, 1963.
[15] A. F. Wright and D. C. Chrzan. *Phys. Rev. Lett.*, 70:1964, 1993.
[16] B. S. Itchkawitz, A. P. Baddor, H. L. Davis, and E.W. Plummer. *Phys. Rev. Lett.*, 68:2488, 1992.

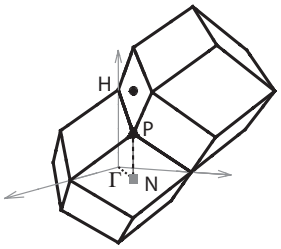

FIG. 1: A particular stacking of two BZ of the bcc structure. Note that $N = \frac{2\pi}{a}\left(0, \frac{1}{2}, \frac{1}{2}\right)$, $H = \frac{2\pi}{a}(0, 0, 1)$, and $P = \frac{2\pi}{a}\left(\frac{1}{2}, \frac{1}{2}, \frac{1}{2}\right)$. The black dot displays the point $\mathbf{q} = \left(\frac{1}{2}\frac{1}{2}1\right)$, which is symmetrically equivalent to the $N-$point phonon.

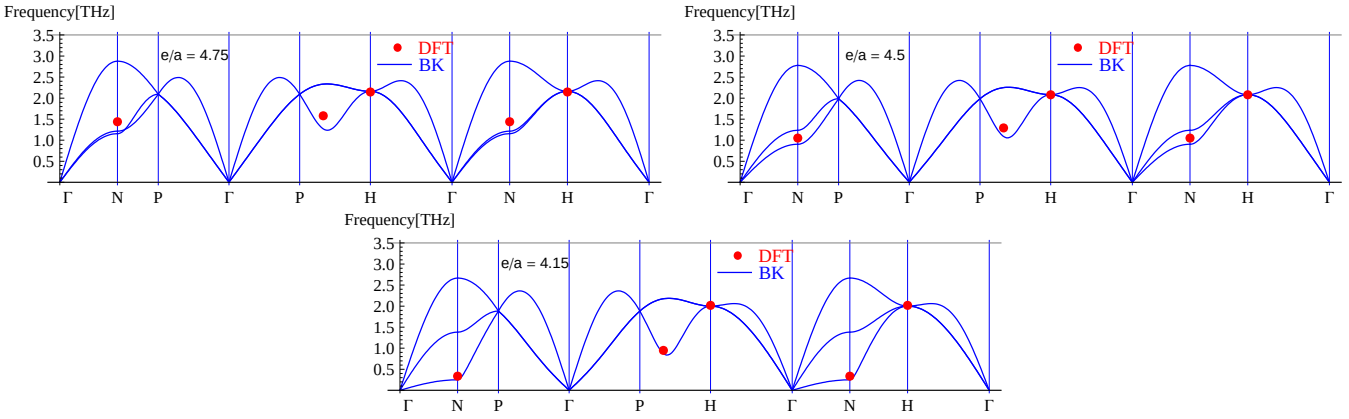

FIG. 2: Dispersion relations over a range of the ratio (e/a) of the Ti-V alloys. The ratio $e/a = 4.75, 4.50$, and 4.15 corresponds to the composition $Ti_{25}V_{75}$, $Ti_{50}V_{50}$, and $Ti_{85}V_{15}$ respectively. The blue lines are the Born-von Karman(BK) harmonic approximations, while the red dots are obtained from the frozen phonon calculations.

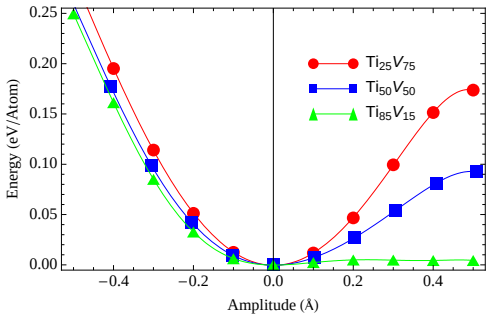

FIG. 3: Total energy of the $\mathbf{q}_\omega-$phonon as a function of displacement amplitude.

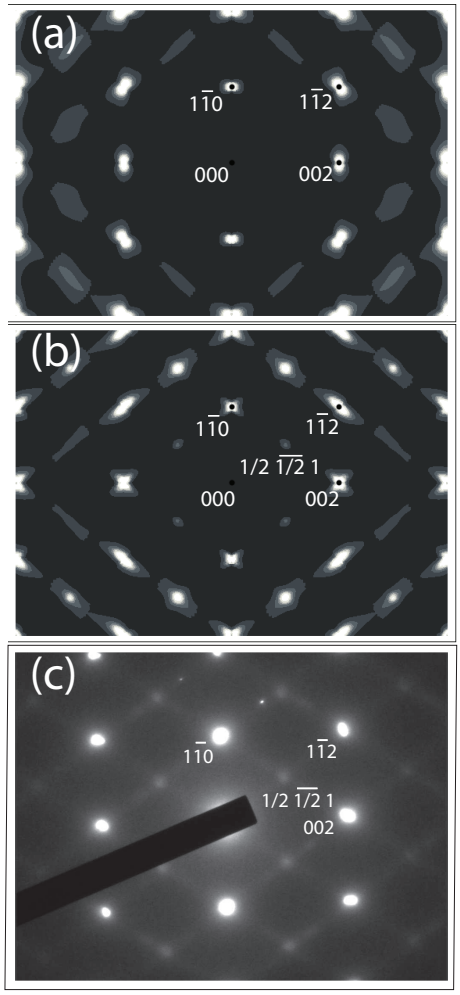

FIG. 4: (a)Theoretical diffraction pattern of $Ti_{25}V_{75}$, and (b)$Ti_{85}V_{15}$. (c)The (110) transmission electron diffraction pattern of solution-treated Gum Metal obtained using transmission electron microscopy.

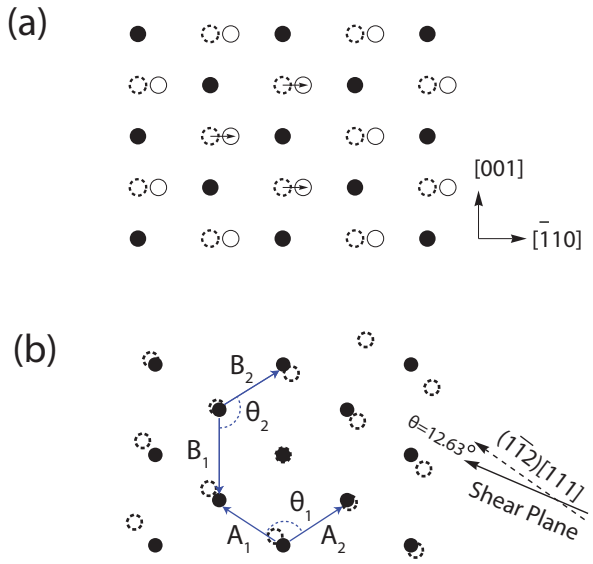

FIG. 5: (a) The transverse $[\frac{1}{2}\frac{1}{2}0]$ mode with the $[1\bar{1}0]$ polarization. The arrows show the direction of the vibration of the alternating planes along [110]. (b)The atomic deformation on the (110) plane due to a long-wavelength shear close to the type $[1\bar{1}1](\bar{1}12)$.